Improved Thermal Design of a Compression Mold

Maria A. Kuczmarski*, J. Christopher Johnston

NASA Glenn Research Center, 21000 Brookpark Road, Cleveland, OH 44135

Abstract

An analysis of the heat transfer in a tool for producing neat resin disks was conducted to determine how to bring about a better agreement between the tool temperature and the applied temperature profile. Using the commercial code FLUENT to investigate the relative effects of heat conduction into the tool and heat loss from the tool by convection, it was shown that convective heat transfer appears more important than conduction in controlling the tool performance. Decreasing the height of the tool was predicted to decrease the heat losses by convection. Redesign of the tool based on this analysis resulted in the tool experiencing the applied temperature profile.

Keywords: computer modeling, high-performance polymers, polyimides, processing

1. Introduction

Development of new high-performance polymer matrix composite materials begins with resin development [1-4]. A common practice is to create a neat resin sample - one with no reinforcing material added - to allow for chemical and mechanical testing to be performed on the cured resin. For high-temperature resins, such as PMR-15 [5] and its

descendents, production of the resin sample requires the application of high temperatures (up to 650 °F) and substantial pressure (several hundreds pounds per square inch) using a specified time-temperature-pressure profile. This requires the resin to be processed in a heated compression tool made of hardened tool steel. The tool is placed into a hydraulic press that supplies the pressure needed for proper resin processing. An example temperature versus time profile is shown in Figure 1. During the first temperature plateau, the imidization reactions are substantially completed. The cross-linking reactions occur during the second temperature plateau.

In normal practice, the temperature feedback is taken from a thermocouple mounted on the side of the tool, as close to the sample as possible. Power is applied to the platen heaters, which contact the tool. The power applied to the heaters is adjusted to minimize the difference between the measured tool temperature and the desired temperature obtained from the programmed profile. In this “part control” mode, the platen temperatures will typically be higher than the profile temperature to offset losses and bring the tool to the desired temperature. For safety reasons, many automated systems limit the maximum difference between the platen and tool temperatures, reducing the power applied to the heating elements once the limit has been reached. For the purposes of this paper, the press was operated in “platen control” mode, where the temperature feedback for the profiles was taken from thermocouples embedded in the platens rather than from the body of the tool itself. This more clearly illustrates the thermal losses in the tool.

While the reproducibility of the platen temperature is generally excellent across runs (Figure 2a), poor reproducibility of the thermal profile applied to the sample can be a problem with commonly available steel tools (Figure 2b). This is despite insulating the

tools with fiberglass and glass cloth. Differences between the platen and tool temperatures can be significant, as shown in Figure 3. Having a minimal temperature difference between the tool and platens results in a more uniform temperature distribution across the tool, assuring that the sample can be heated according to the programmed temperature profile. This also results in a minimum temperature difference across the sample, yielding proper resin processing and uniform sample properties.

A thermal analysis of a typical commercially-obtained tool was undertaken to determine how to minimize the temperature difference between the tool and the platens. A computational model was used to analyze the system and investigate proposed changes. Based on the results, a re-designed tool was constructed and tested that significantly decreased thermal losses as evidenced by minimal temperature differences between the platen and tool.

2. Experimental Method

The polymer used for these tests was imidized PMR-15 resin obtained from HyComp, Inc. PMR-15 is a polyimide polymer that cross-links through the endcaps to form a high-temperature polymer with good mechanical strength. The imidized powder (often referred to as molding powder) has been reacted to form oligomers with an average molecular weight of approximately 1500 g/mole. This powder is further processed at high temperature to yield the final, cross-linked material.

Figure 4a shows the commercially-obtained tool that was investigated. It consists of a base, body, and punch. After the parts of the tool are coated with a release agent, the base and body are assembled. These parts are designed so that after assembly, the base

extends a short distance into the tool body. The punch is made long enough so that it can protrude through the bottom of the body to facilitate disassembly. During use, the material to be processed -- 0.2 g of PMR-15 molding powder -- is placed on the top face of the base and is contained by the body. The punch is then placed into the body in contact with the molding powder. Because the components of the tool are often stuck together at the end of a run by a thin film of processed resin, the difference in diameter allows the tool body to be supported while the punch pushes out the tool bottom and the sample. The tool can then be inverted and the punch pushed out in a similar manner.

PMR-15 resin disk processing typically requires that pressure not be applied until the upper hold temperature is reached. Since the hydraulic pressure of the press is not regulated accurately enough to provide contact with the punch top without applying pressure, a mechanical stop is used, as shown in Figure 4b. This must be removed before pressure can be applied, which disturbs the insulation around the tool and causes a change in the thermal environment. The assembled tool and mechanical stop are placed on a steel force spreader plate on the lower platen of the press. The spreader plate prevents damage to the platens by the much harder tool. The stop is adjusted to create about a 0.25” gap between the top punch surface and the bottom of the upper platen. A second force spreader plate is placed on top of the tool and stop and the press closed. The tool and stop are then surrounded by insulation consisting of a mixture of glass cloth and fiberglass batting, which is in contact with both the upper and lower platens. A type “J” thermocouple is attached to the midpoint of the tool and another is placed into the air gap between the top of the punch and the upper platen. The upper and lower platens are heated following the

programmed profile and the temperatures of the platens, body, and air gap are automatically recorded.

For this paper, all experimental runs were performed in a heated platen hydraulic press open to the air. The same temperature and pressure profiles were used for all runs. CSS200 software from AvPro, Inc. was used to create and execute time-temperature profiles, while monitoring the temperature on the outer tool body surface.

3. Computational Model

A study bracketing several important input parameters was conducted because it was deemed to provide better insight on how to improve the tool performance than a detailed model with the exact inputs for a specific tool. It was assumed that a number of simplifications could be made that would still result in valid characterization of the tool performance. Through the use of two models, one of the un-insulated tool, and one of a simplified insulation touching only the outermost part of the tool (see Figure 4a), the performance of the tool should be bracketed. In a similar way, by choosing a typical range of heat transfer coefficients for cooling in air [6], the effects of convective heat transfer can be bracketed. Through this type of analysis, information may be obtained to better understand the tool performance. The spreader plates, being only one-quarter inch in thickness and made of steel, were initially assumed to come quickly to the temperature of the platens, and were not included in the model. Finally, radiation heat transfer was neglected.

The computational fluid dynamics code FLUENT [7] was used for the models. It uses a finite volume method to discretize the continuity, momentum, and energy equations, and

can be used to solve any of these equations, alone or combination. In this study it was used to study the heat transfer by conduction in the tool and by convection to the surrounding environment.

The energy transport equation used by FLUENT in solid regions is given by [7] :

$$\frac{\partial(\rho h)}{\partial t} + \nabla \cdot (\vec{v}\rho h) = \nabla \cdot (k \nabla T) + S_h \qquad (1)$$

Where: ρ = density (kg/m^3)

h = sensible enthalpy (J/kg)

k = conductivity (W/m K)

T = temperature (K)

S_h = volumetric heat source (W/m^3)

In this model, three of the four terms in equation (1) drop out: 1) the first term on the left hand side, since a steady state, rather than time-dependent, solution was used; 2) the second term on the left side of the equation, since the solid is stationary; 3) the second term on the right side of the equation, since there is no volumetric heat source.

Figure 5a shows a dimensioned drawing of the commercially-obtained tool. Figures 5b and c show the portion of the uninsulated and insulated tool modeled. When insulation was used, it was axisymmetric around the tool. Symmetry was utilized to allow modeling of only half of the tool, thereby saving on the computational time required. The centerline was defined as an axis boundary type in FLUENT. This was placed along the x-axis as required by the code to allow the two-dimensional axisymmetric form of the equations to be solved. A non-uniform grid was used over portions of the model in order to minimize the number of computational cells needed. The maximum aspect ratio used for the cells

was 5:1. A temperature profile consisting of the following steps was applied to both the top and bottom walls:

1. A temperature ramp of 0.0463 K/s for 3300 s.
2. A hold at 449.8 K for 1800 s.
3. A temperature ramp of 0.0463 K/s for 3000 s.
4. A hold at 588.7 K for 3600 s.
5. A temperature ramp of -0.0463 K/s for 6300 s.

The side walls were defined as having a convection boundary condition with a free-stream temperature of 293 K. Heat transfer coefficients of 1, 25, and 50 W/m^2 K were used. Predicted temperatures were taken from a point corresponding to the location of experimental temperature measurements, as shown in Figure 5b.

A second-order upwind scheme was used for the energy equations. The under-relaxation factor for energy was set to 1. The solution was considered to have converged when the scaled residuals for the energy equation dropped below $1x10^{-6}$; further reductions did not change the predicted values for temperature. All transient calculations used a time step of 60 s. Data files were saved every five time steps.

Three different grid densities were examined to determine the sensitivity of the results to the grid density. Table 1 shows the grid densities used for both the uninsulated and insulated tool models. The difference in temperatures at corresponding time steps between grid 1 and grid 2 was generally less than 1%, with a maximum difference of 1%. The shape and overlap of the curves was similar for heat transfer coefficients of 25 and 50

W/m^2 K. The difference in temperatures between grid 2 and grid 3 was generally less than 1%, with a maximum difference of 1.7%. For the insulated tool with a heat transfer coefficient of 1 W/m^2 K, the difference in temperatures between grid 1 and grid 2 was always less than 1%, with a maximum difference of 0.8%. For grid 2 and grid 3, the temperature difference was generally less than 1%, with a maximum difference of 1.3%. The shape and overlap of the curves was similar for heat transfer coefficients of 25 and 50 W/m^2 K. Based on these results, grid 1 was deemed sufficient and used for the rest of the computational runs described.

A re-designed tool was also modeled. A dimensioned drawing is shown in Figure 6a and the portion of the uninsulated and insulated tool that was modeled is shown in Figures 6b and c. When insulation was used, it was axisymmetric around the tool. Again, symmetry was used to decrease the model size. A grid sensitivity study was performed with the grid densities shown in Table 2. The predicted temperature difference between grid 1 and grid 2 and between grid 2 and grid 3 was less than 1%, so grid 1 was used for further work. Predicted temperatures were taken from a point corresponding to the location of experimental temperature measurements, as shown in Figure 6b.

4. Results and Discussion

An analysis was first performed on the commercially-obtained tool. Figure 7 show a representative experimental measurement of the tool and platen temperatures, along with the predicted temperatures from the model for the insulated tool and for the uninsulated tool with three different heat transfer coefficients. The insulated tool showed virtually no difference in the predicted temperatures when the heat transfer coefficient was varied. The

uninsulated model and insulated model bracket the performance of the actual tool, showing that conclusions drawn from results from these two models may be used to guide improvements to the tool performance.

The heat transfer by conduction in a two-dimensional problem may be described by [8]:

$$Q_{conduction} = -kA_{conduction}\left(\frac{\partial T(x,y,t)}{\partial x}\right) \quad (2)$$

Where: $Q_{conduction}$ = rate of heat flow by conduction (W)

k = thermal conductivity (W/m K)

$A_{conduction}$ = area of heat flow (m^2)

T = temperature (K)

The heat transfer by convection may be described as [8]:

$$Q_{convection} = hA_{convection}\left(T_{surface} - T_{\infty}\right) \quad (3)$$

Where: $Q_{convection}$ = rate of heat flow by convection (W)

h = heat transfer coefficient (W/m^2 K)

$A_{convection}$ = area of heat flow (m^2)

$T_{surface}$ = surface temperature (K)

T_{∞} = free stream temperature (K)

The above equations suggests that altering the thermal conductivity, heat transfer coefficient, and the areas available for heat transfer could all be investigated as methods for

bringing the platen and tool temperatures into closer agreement. Thermal conductivity would be related to the material used to manufacture the tool, the heat transfer coefficient would be related to the environment surrounding the tool, and the surface area for heat transfer would be related to the geometry of the tool or tool-insulation combination.

The effects of varying the thermal conductivity of the tool material, as well as the heat transfer coefficient, were examined. Figure 8 shows the predicted tool temperatures over time for the insulated and uninsulated tool for three different materials with greatly differing thermal conductivities, using three different values for the heat transfer coefficient. While neither copper nor aluminum is hard enough for long-term use as tool materials, they were used to illustrate the effect of varying thermal conductivity and, therefore, conductive heat transfer into the tool. The insulated tool model predicts nearly identical temperature curves for all thermal conductivities and heat transfer coefficients, as shown in Figures 8a, b, and c. So, in this configuration, changes in either the thermal conductivity or heat transfer coefficient will not significantly affect the tool temperature. Figures 8d, e, and f show that in the uninsulated tool, increasing the thermal conductivity of the tool material decreases the relative importance of convective heat transfer, likely because heat can be more efficiently supplied to the tool to keep up with convective losses. Since the actual tool performance lies somewhere between the insulated and uninsulated model, a combination of increasing the thermal conductivity of the tool material and decreasing the heat loss by convection would bring the platen and tool temperatures into better agreement. However, in practical application, the tool material cannot be easily altered. For long life at the pressures applied, hardened steel is the best material.

Therefore, reducing heat transfer by convection will be the focus of the remainder of the study.

To compare the effect of the surface area on the two modes of heat transfer, we looked at the ratio of the surface area through which heat is supplied to the tool to the surface area available for convective heat loss. If the shape of the tool is approximated as a cylinder, the surface area through which heat is supplied to the tool would be the top and bottom of the ends of a cylinder:

$$\text{Surface area for heat conduction into cylinder} = 2\left(\pi \times r^2\right) \quad (4)$$

Where: r = tool radius (m)

The surface area available for convective heat transfer for a cylinder is:

$$\text{Surface area for convective heat transfer} = 2\pi \times rH \quad (5)$$

Where: H = tool height (m)

The ratio of the two yields:

$$\frac{\text{Surface area for heat conduction into cylinder}}{\text{Surface area for convective heat transfer}} = {}^{r}\!/_{H} \quad (6)$$

This implies that the platen and tool temperatures could be brought closer together either by increasing the radius of the tool (increasing heat conducted into the tool) or decreasing the height of the tool (decreasing heat lost by convective heat transfer). Increasing the radius of the tool increases the mass of the punch, which is an issue with low viscosity resins that can be pushed out of the tool by the weight of the punch alone.

A new tool was designed with the height reduced from 59.1 mm to 40.1 mm. The radius of the re-designed tool was made as large as possible without the new punch exceeding the mass of the original punch. A calculation of the ratio of surface area for convection to that for conduction shows a value of 5.5 for the original, uninsulated tool and 1.3 for the re-designed tool, indicating that convective heat losses should be reduced in this new design. Figure 9a shows the predicted temperatures for the uninsulated re-designed tool for three heat transfer coefficients. The results are nearly identical, indicating the decreased importance of convective heat transfer with this configuration. There was no observable difference between the curves for the insulated version of the re-designed tool, as shown in Figure 9b.

Based on these results, the re-designed tool was built and tested. A comparison of the performance of the re-designed tool compared to the old is shown in Figure 10. In Figure 10a, the insulation was removed midway during the run to indicate the performance of an uninsulated tool. Figure 10b shows the performance of the re-designed tool run with and without insulation. The performance of the re-designed uninsulated tool matches that of the old insulated tool. With insulation, the re-designed tool results in the smallest difference between platen and tool temperatures. Compared to the repeatability of the old tool temperature, shown in Figure 2b, the re-designed tool design has increased the

repeatability of the tool temperature from run to run, as shown in Figure 11. While one run shows an abrupt drop at the end of the upper temperature plateau due to equipment problems, it is complete enough to show the repeatability of the tool temperature.

Figure 12 shows temperature contours in both the old and new tool designs for cases with the side wall convective heat boundary condition using a heat transfer coefficient of 25 W/m^2 K. The temperature distribution across the new tool design is smaller compared to that in the old tool design, less than 10 K compared to almost 20 K. In addition, a more uniform temperature distribution exists across the sample in the new tool design, 2 K compared to 8 K in the old tool design. The smaller the temperature difference across the sample, the more uniform the resin properties, since reaction rates and viscosities are temperature dependent.

5. Conclusions

The results of this study showed that convective heat losses negatively impacted the performance of a commercially-obtained tool, as evidenced by significant temperature difference between the temperature applied to the platens and the tool temperature. Increasing the thermal conductivity of the tool, while likely not practical, results in the tool being less sensitive to convective heat transfer. Decreasing the surface area available for convective heat transfer was shown to be a viable method for decreasing the losses, minimizing the temperature difference between the tool and platen temperatures. The analysis led to the design of a re-designed tool, which resulted in a significantly smaller difference between platen and tool temperatures, and, therefore, smaller losses and improved reproducibility. The computational portion of the work guided the re-design of

the tool, saving time and money by preventing the pursuit of apparently reasonable, but ultimately ineffective, concepts.

Processing of materials is often done on a trial-and-error basis, simply altering parameters until values that work reasonably well are found. While this may work adequately in the early stages of process development, a proper understanding of the transport processes involved in the system can provide information that allows the process to be more efficiently fine tuned to produce the required performance. Such information may be obtained through a theoretical and/or computational approach to optimize the system performance. This study is an example of the types of analysis that can be applied to materials process development, and the power of a coordinated computational/experimental approach to process optimization.

Acknowledgements

Financial support from the NASA Low Emissions Alternative Power Program is gratefully acknowledged. We thank DeNise Hardy-Green for her efforts in testing the redesigned tool and Dr. Robert Miller for his helpful discussions about the analysis of the modeling.

6. References

1. Meador, M.A., Johnston, J.C., Cavano, P.J, Frimer, "Oxidative Degredation of Nadic-End-Capped Polyimides. 2. Evidence for Reactions Occurring at High Temperatures," Macromolecules, 30, 1997, 3215-3223.

2. Turk, M.J., Ansari, A.S, Alston, W.B., Gahn, G.S., Frimer, A.A., Scheiman, "Evaluation of the Thermal Oxidative Stability of Polyimides via TGA Techniques," J. Polymer Science: Part A.: Polymer Chemistry, 37, 1999, 3943- 3956.

3. Wan, Q., Rumpf, D., Schricker, S.R., Mariotti, A., Culbertson, B.M., "Influence of Hyperbranched Multi-Methacrylates for Dental Neat Resins on Proliferation of Human Gingival Fibroblasts," Biomacromolecules, 2, 2001, 217-222.

4. Hou, T.H., "Processing Robustness for a Phenylethynl-Terminated Polyimide Composite," J. Applied Polymer Science, 100, 2006, 3212-3221.

5. T.T. Serafini, P. Delvigs, G.R. Lightsey, "Thermally Stable Polyimides from Solutions of Monomeric Reactants," J. Applied Polymer Science, 16, 1972, 905-915.

6. McCabe, W.L., Smith, J.C., Unit Operations of Chemical Engineering, 3rd ed., McGraw-Hill Book Company, New York, 1976, p 302.

7. FLUENT, version 6.2.16, Fluent, Incorporated, Hanover, NH.

8. Ozisik, M.N., Heat Transfer: A Basic Approach, McGraw-Hill Book Company, New York, 1985, P.2, 6, 25

Figure Captions

Figure 1: Typical time-temperature profile applied to the platens.

Figure 2: Commercially-obtained tool: a) Repeatability of platen temperatures across runs; b) repeatability of tool temperature across runs.

Figure 3: Commercially-obtained tool: comparison of platen and tool temperatures.

Figure 4: Commercially-obtained tool: a) Diagram showing a simplified application of insulation as used in the model; b) tool and mechanical stop.

Figure 5: Commercially-obtained tool: a) Dimensioned diagram; b) diagram of uninsulated model, with location of thermocouple indicated; c) diagram of insulated model.

Figure 6: Re-designed tool: a) Dimensioned diagram; b) diagram of uninsulated model, with location of thermocouple indicated; c) diagram of insulated model.

Figure 7: Commercially-obtained tool: representative experimental measurements of platen and tool temperatures, predicted temperature from insulated model, and predicted temperatures from the uninsulated model for three different heat transfer coefficients.

Figure 8: Commercially-obtained tool: predicted tool temperatures for three different heat transfer coefficients for an: a) insulated steel tool; b) insulated aluminum tool; c) insulated copper tool; d) uninsulated steel tool; e) uninsulated aluminum tool; f) uninsulated copper tool.

Figure 9: Re-designed tool: predicted tool temperatures for three different heat transfer coefficients for: a) uninsulated tool; b) insulated tool.

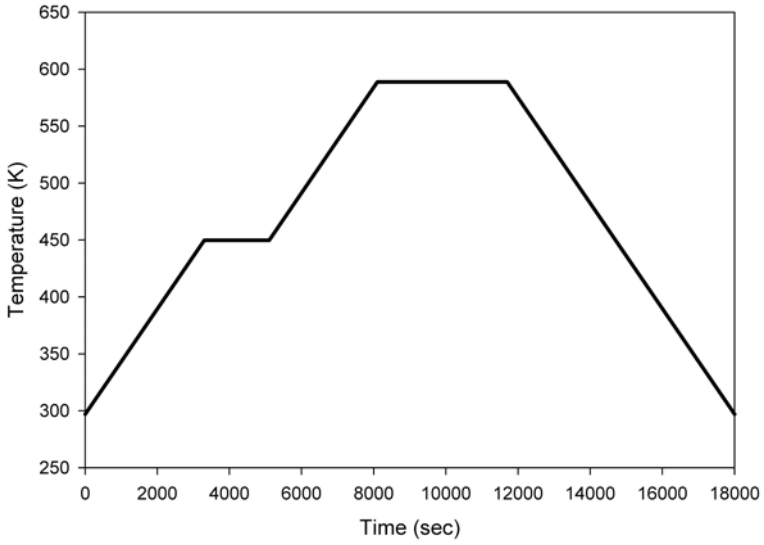
650
600
550
500
450
400
350
300
250
Temperature (K)
0
2000
4000
6000
8000
10000
12000
14000
16000
18000
Time (sec)

Figure 1

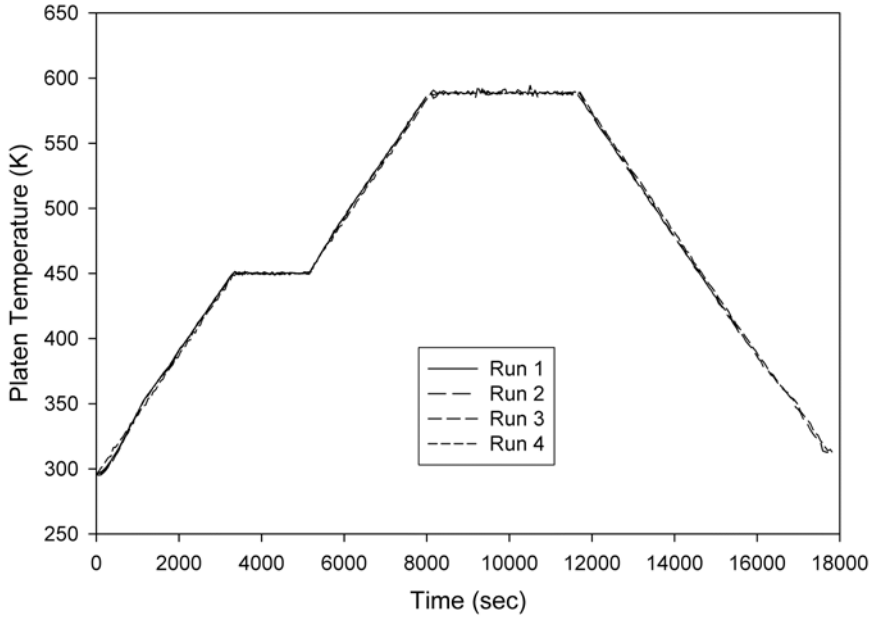
Platen Temperature (K)
650
600
550
500
450
400
350
300
250
0
2000
4000
6000
8000
10000
12000
14000
16000
18000
Time (sec)
Run 1
Run 2
Run 3
Run 4

a)

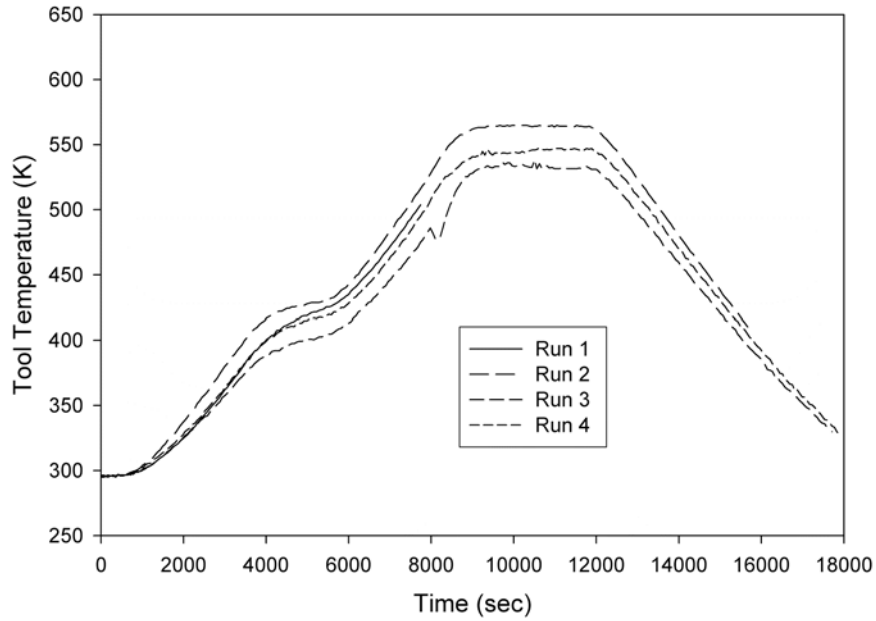
Tool Temperature (K)
650
600
550
500
450
400
350
300
250
0
2000
4000
6000
8000
10000
12000
14000
16000
18000
Time (sec)
Run 1
Run 2
Run 3
Run 4

b)

Figure 2

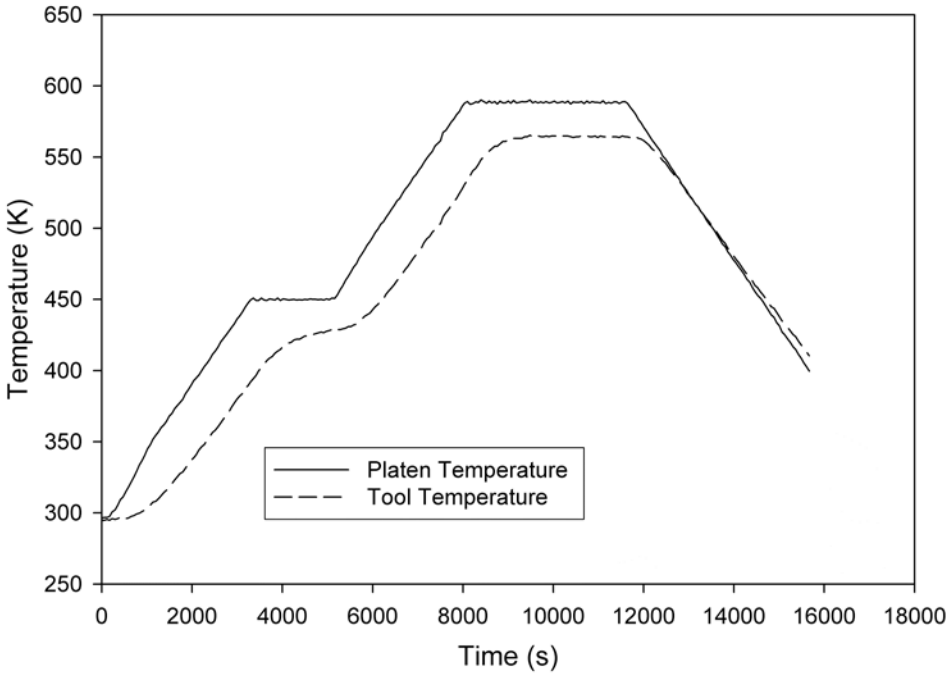
650
600
550
500
450
400
350
300
250
Temperature (K)
0
2000
4000
6000
8000
10000
12000
14000
16000
18000
Time (s)
Platen Temperature
Tool Temperature

Figure 3

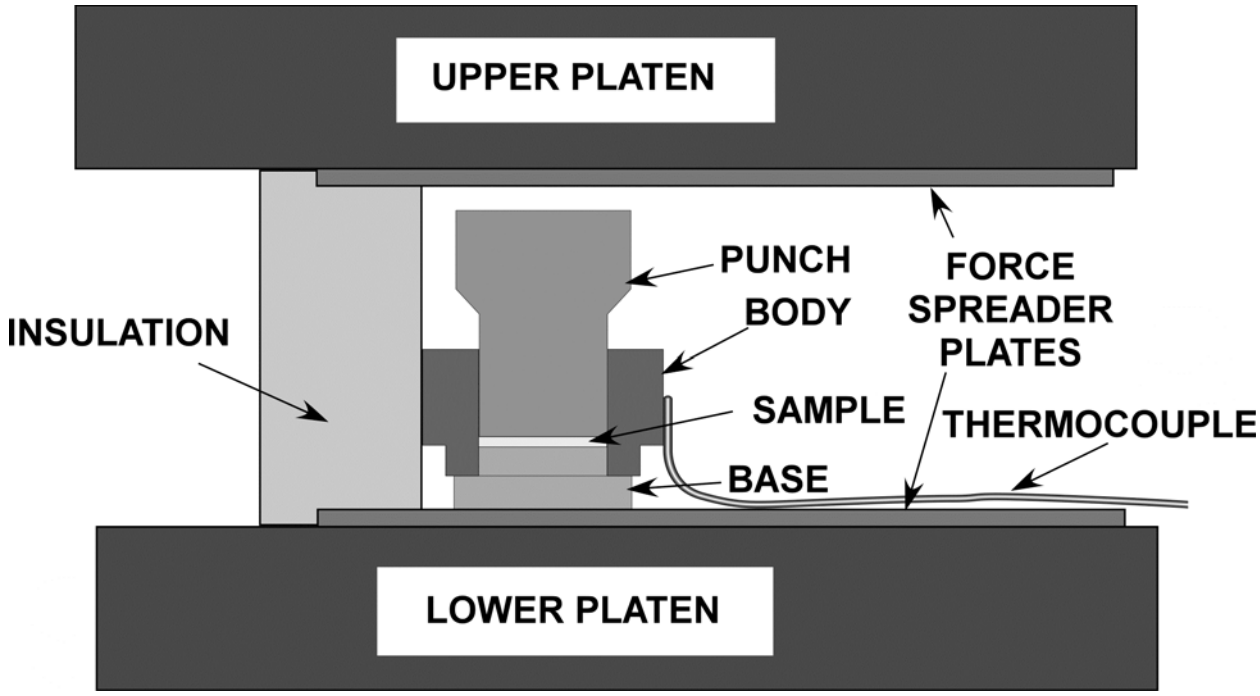
UPPER PLATEN
PUNCH
BODY
FORCE
SPREADER
PLATES
INSULATION
SAMPLE
THERMOCOUPLE
BASE
LOWER PLATEN

a)

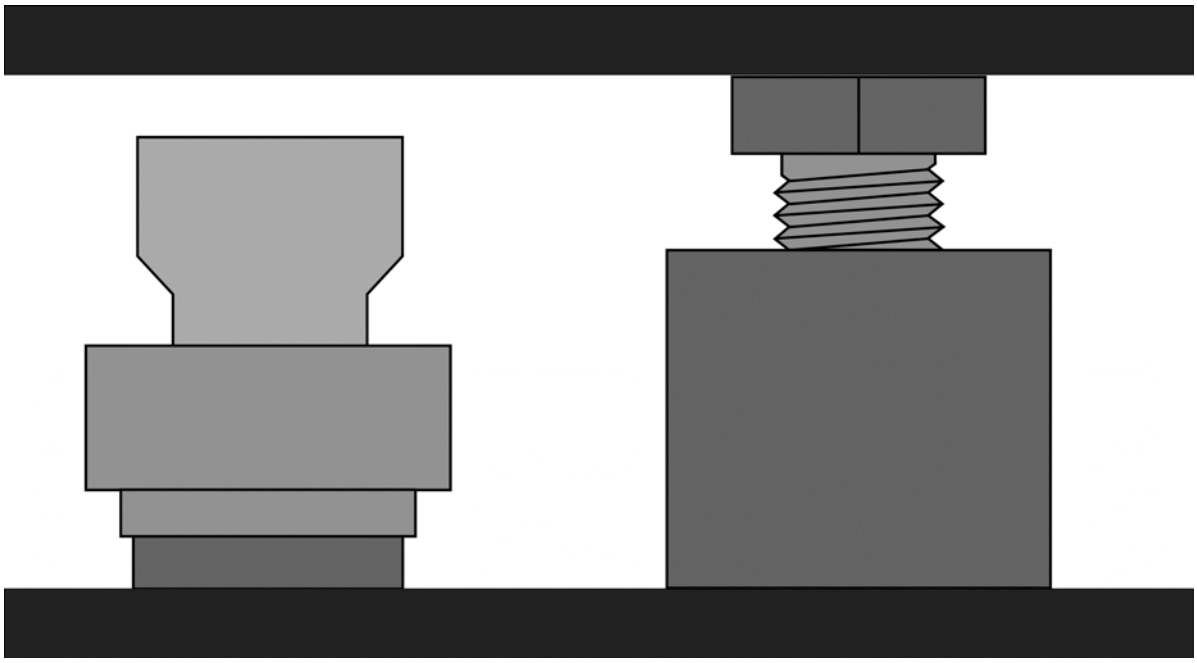

b)

Figure 4

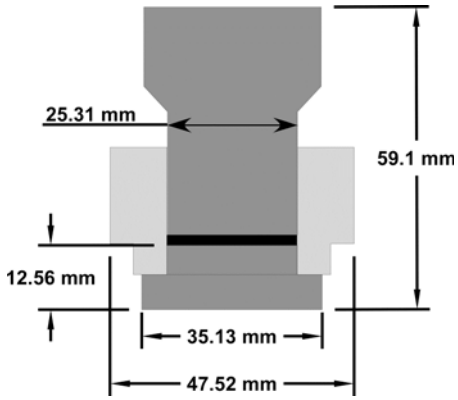
25.31 mm
59.1 mm
12.56 mm
35.13 mm
47.52 mm

a)

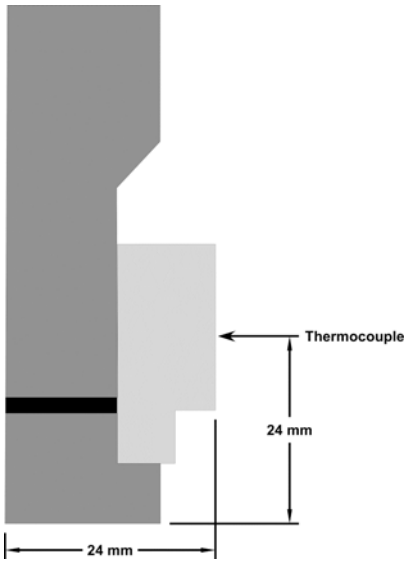
Thermocouple
24 mm
24 mm

b)

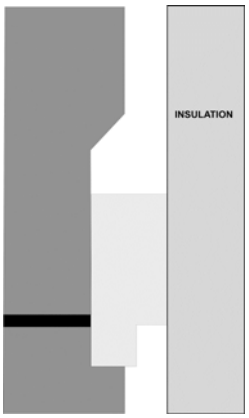
INSULATION

c)

Figure 5

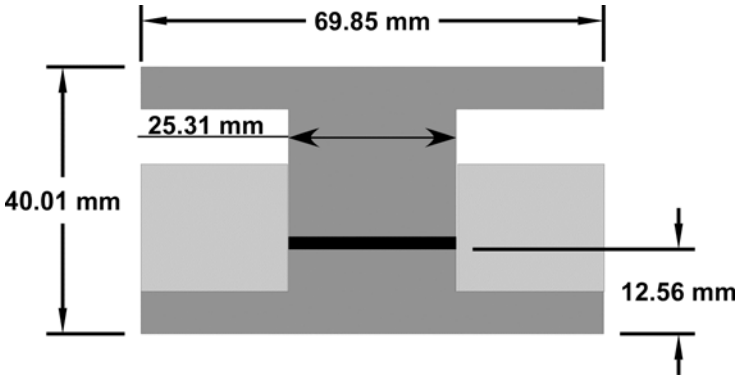
69.85 mm
25.31 mm
40.01 mm
12.56 mm

a)

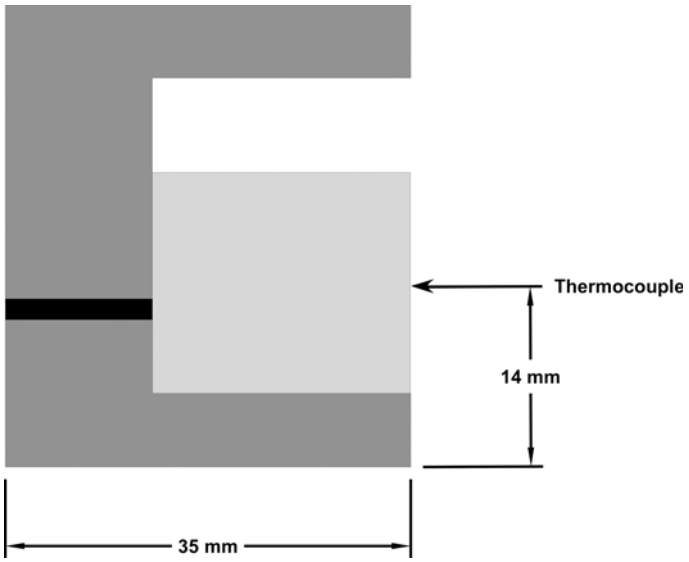
Thermocouple
14 mm
35 mm

b)

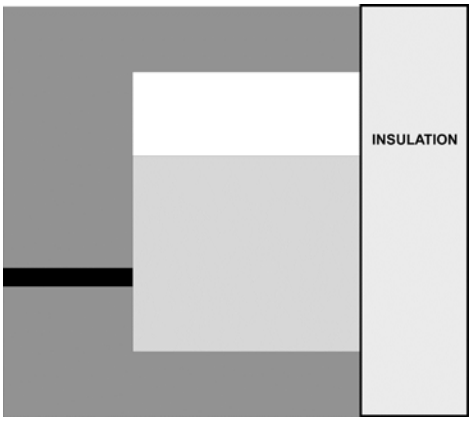
INSULATION

c)

Figure 6

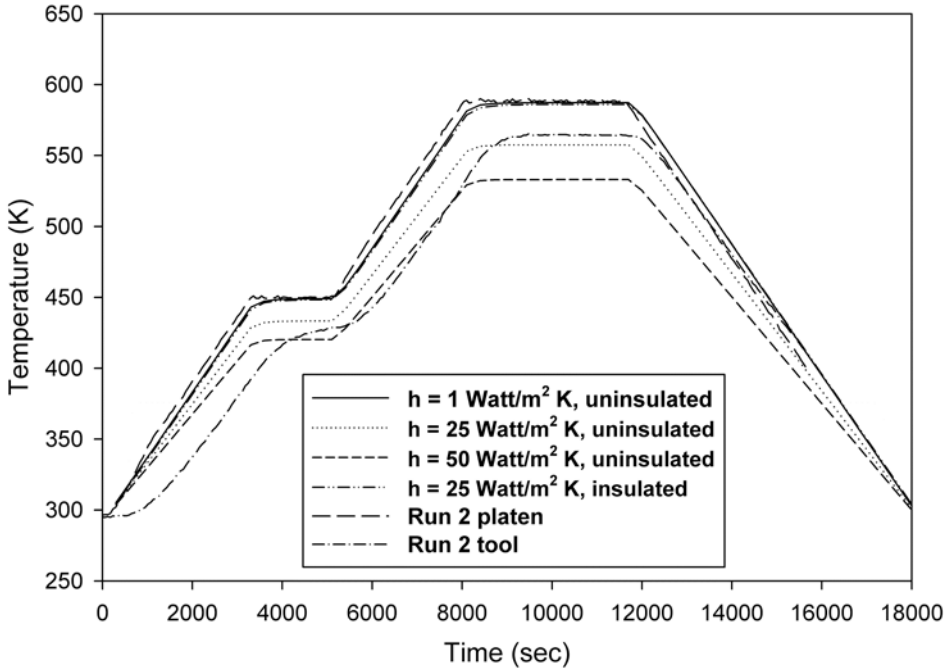
650
600
550
500
450
400
350
300
250
Temperature (K)
0
2000
4000
6000
8000
10000
12000
14000
16000
18000
Time (sec)
h = 1 Watt/m2 K, uninsulated
h = 25 Watt/m2 K, uninsulated
h = 50 Watt/m2 K, uninsulated
h = 25 Watt/m2 K, insulated
Run 2 platen
Run 2 tool

Figure 7

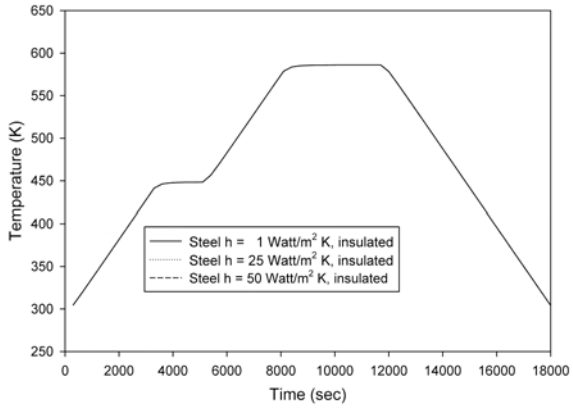

a)

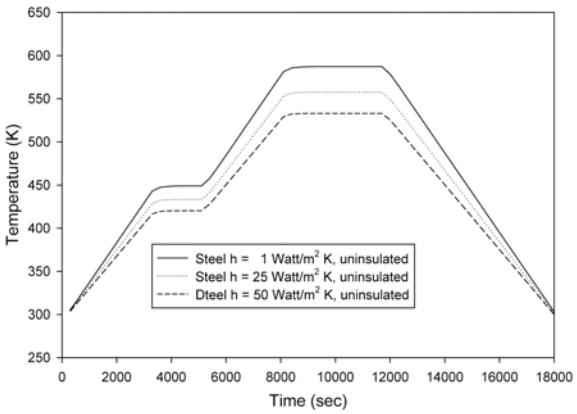

d)

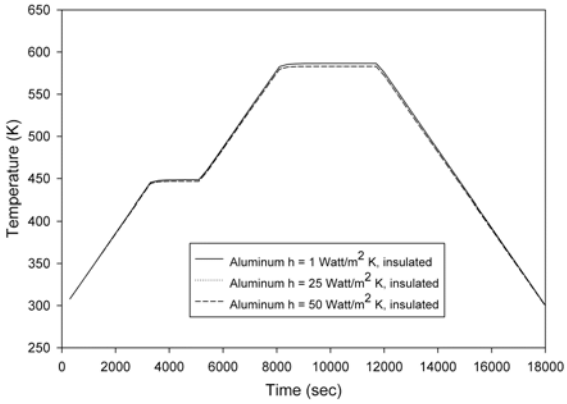

b)

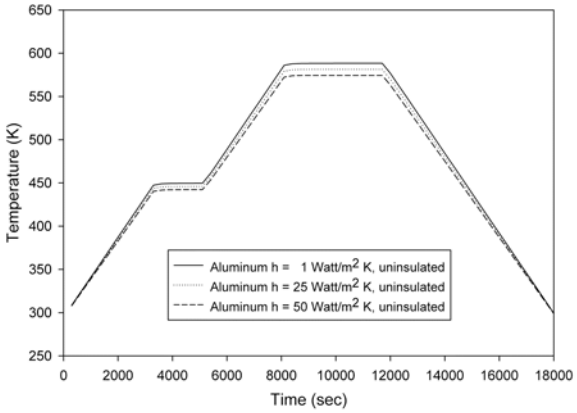

e)

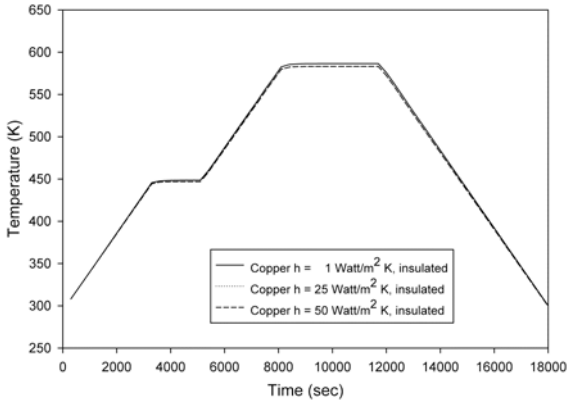

c)

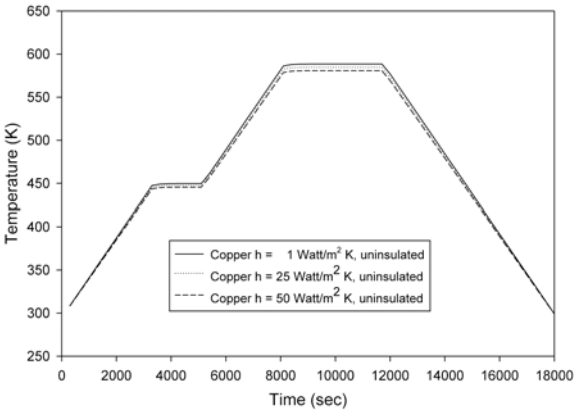

f)

Figure 8

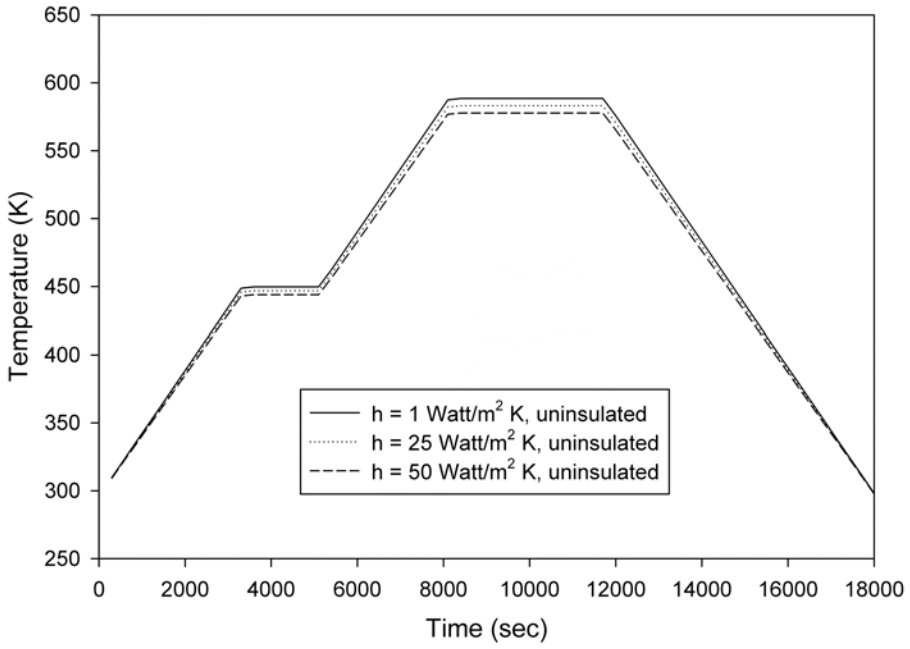
650
600
550
500
450
400
350
300
250
Temperature (K)
0
2000
4000
6000
8000
10000
12000
14000
16000
18000
Time (sec)
h = 1 Watt/m2 K, uninsulated
h = 25 Watt/m2 K, uninsulated
h = 50 Watt/m2 K, uninsulated

a)

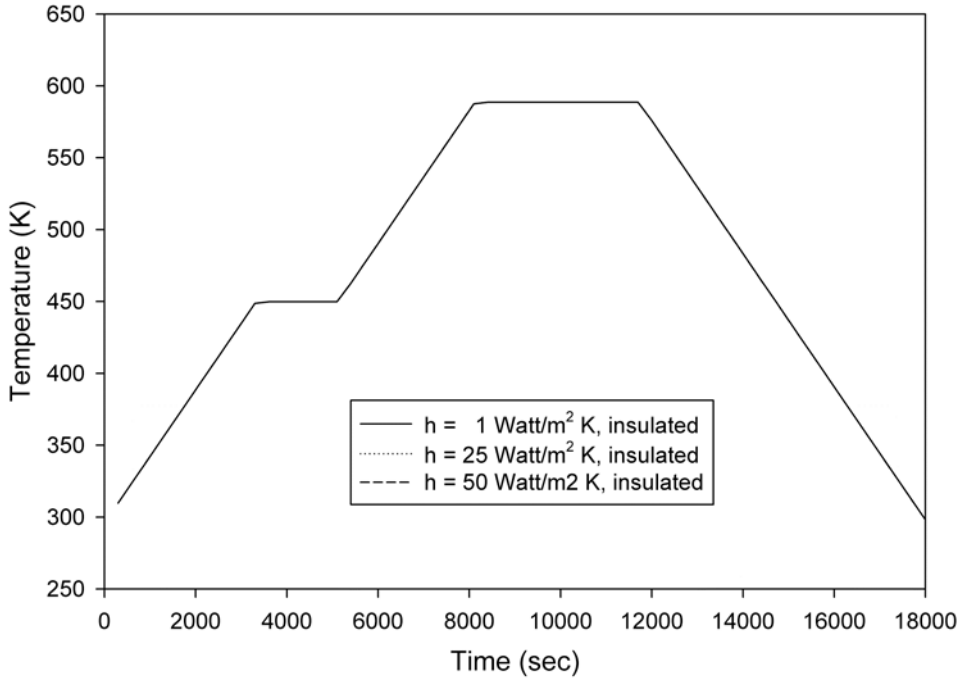
650
600
550
500
450
400
350
300
250
Temperature (K)
0
2000
4000
6000
8000
10000
12000
14000
16000
18000
Time (sec)
h = 1 Watt/m2 K, insulated
h = 25 Watt/m2 K, insulated
h = 50 Watt/m2 K, insulated

b)

Figure 9

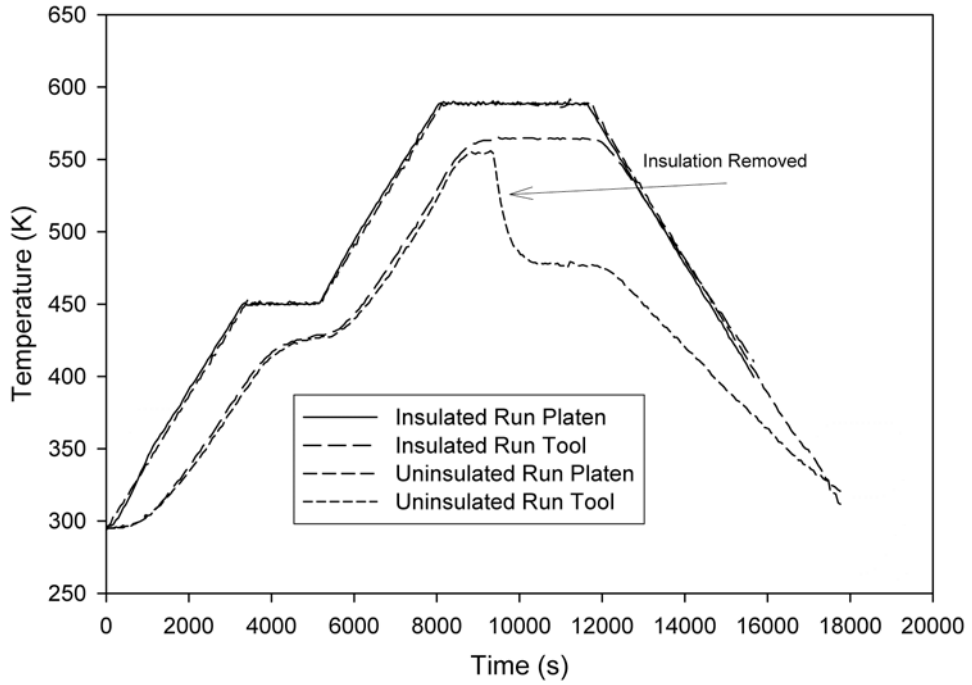
650
600
550
500
450
400
350
300
250
Temperature (K)
0
2000
4000
6000
8000
10000
12000
14000
16000
18000
20000
Time (s)
Insulation Removed
Insulated Run Platen
Insulated Run Tool
Uninsulated Run Platen
Uninsulated Run Tool

a)

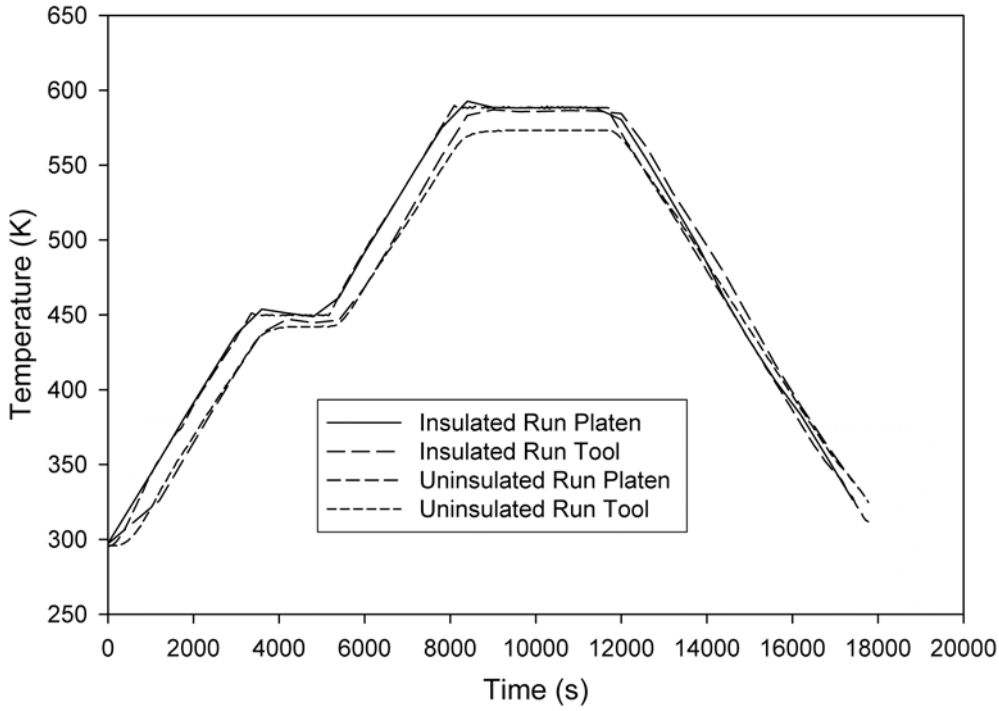
650
600
550
500
450
400
350
300
250
Temperature (K)
0
2000
4000
6000
8000
10000
12000
14000
16000
18000
20000
Time (s)
Insulated Run Platen
Insulated Run Tool
Uninsulated Run Platen
Uninsulated Run Tool

b)

Figure 10

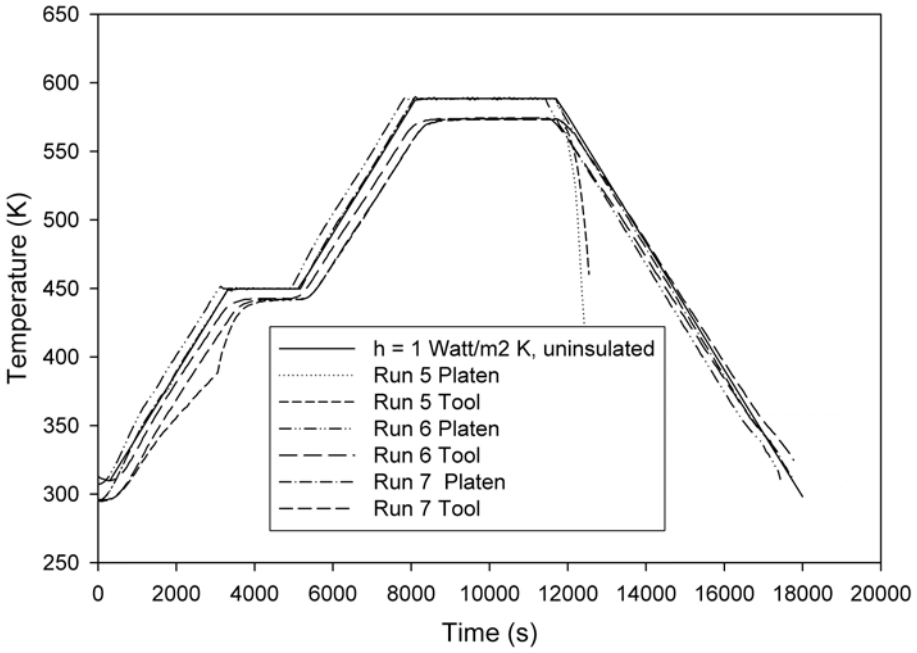
650
600
550
500
450
400
350
300
250
Temperature (K)
0
2000
4000
6000
8000
10000
12000
14000
16000
18000
20000
Time (s)
h = 1 Watt/m2 K, uninsulated
Run 5 Platen
Run 5 Tool
Run 6 Platen
Run 6 Tool
Run 7 Platen
Run 7 Tool

Figure 11

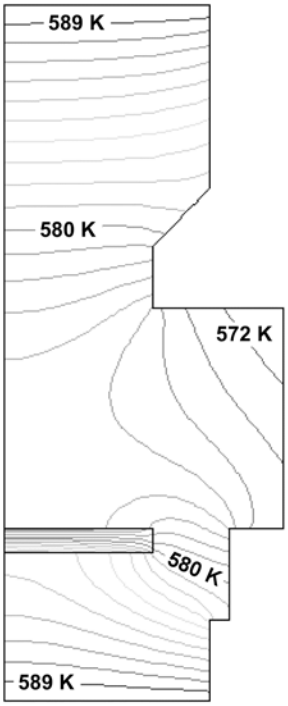

a)

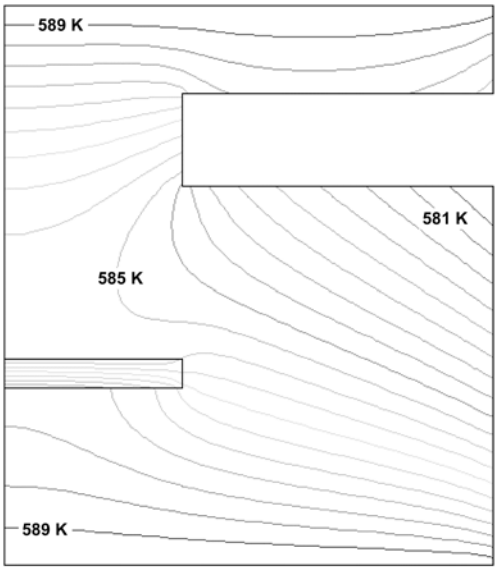

b)

Figure 12

Table 1: Grid Densities Examined for Commercially-Obtained Tool Model

	Tool without Insulation		Tool with Insulation	
	Number of Cells in X-Direction	Number of Cells in Y-Direction	Number of Cells in X-Direction	Number of Cells in Y-Direction
Grid 1	96	36	96	51
Grid 2	194	70	194	100
Grid 3	289	105	289	150

Table 2: Grid Densities Examined for Re-Designed Tool

	Re-Designed Tool (without insulation)	
	Number of Cells in X-Direction	Number of Cells in Y-Direction
Grid 1	58	52
Grid 2	120	103
Grid 3	177	154